Analytical and Finite Element Analysis for Demagnetization Fault of External Rotor PMSM

Ahmed Belkhadir, Remus Pusca, Raphaël Romary, Driss Belkhayat, Youssef Zidani, Abderrahmane Rebhaoui

Analytical and Finite Element Analysis for Demagnetization Fault of External Rotor PMSM

Ahmed Belkhadir *
Univ. Artois, UR 4025, Laboratoire Systèmes Electrotechniques et Environnement (LSEE), F-62400 Béthune, France.
Univ. Cadi Ayyad, P.O. Box 549, Laboratoire des Systèmes Electriques, Efficacité Energétique et Télécommunications (LSEEET), Marrakesh, Morocco.
ahmed_belkhadir@ens.univ-artois.fr
ahmed.belkhadir@ced.uca.ma

Remus Pusca
Univ. Artois, UR 4025, Laboratoire Systèmes Electrotechniques et Environnement (LSEE), F-62400 Béthune, France.
remus.pusca@univ-artois.fr

Raphaël Romary
Univ. Artois, UR 4025, Laboratoire Systèmes Electrotechniques et Environnement (LSEE), F-62400 Béthune, France.
raphael.romary@univ-artois.fr

Driss Belkhayat
Univ. Cadi Ayyad, P.O. Box 549, Laboratoire des Systèmes Electriques, Efficacité Energétique et Télécommunications (LSEEET), Marrakesh, Morocco.
driss.belkhayat@uca.ma

Youssef Zidani
Univ. Cadi Ayyad, P.O. Box 549, Laboratoire des Systèmes Electriques, Efficacité Energétique et Télécommunications (LSEEET), Marrakesh, Morocco.
y.zidani@uca.ma

Abderrahmane Rebhaoui
Univ. Artois, UR 4025, Laboratoire Systèmes Electrotechniques et Environnement (LSEE), F-62400 Béthune, France.
abderrahmane.rebhaoui@vedecom.fr

***Abstract*— Various factors can lead to the demagnetization of permanent magnets, such as excessive magnetomotive force and/or high operating temperatures. As a result, the machine's flux density distribution is no longer uniform, producing new fault harmonics and reducing motor efficiency. In view of this problem, this paper presents the behavior of an external rotor permanent magnet synchronous machine in the presence of a total demagnetization fault in two adjacent magnets. The machine's performance will be evaluated using an analytical model that has been developed. Finite element analysis and experiment tests are used to validate the feasibility of the proposed analytical model.**

Keywords— Demagnetization fault, external rotor permanent magnet synchronous machine, analytical model, finite element analysis.

I. INTRODUCTION

External Rotor Permanent Magnet Synchronous Motors (ER-PMSMs) is a topology that can be suitable in Hybrid and Electric Vehicles (HEV) driven by motors integrated into the vehicle wheels. The drive form that uses this type of machine can be the future trends due to the advantages of a compact drive system, high efficiency, effectiveness and good control performance. However, ER-PMSMs are sensitive to various types of faults that can decrease the stability and driving comfort of the vehicle or bring the system to a complete shutdown.

Permanent Magnet (PM) are sensitive to inter-turn short circuit faults, manufacturing problems or excessive temperature variation, which can cause complete or partial Demagnetization Faults (DF) in a certain region of the rotor pole. This type of fault can lead to a reduction or unbalance magnetic flux, mechanical vibration or decrease of the torque and the efficiency of the ER-PMSM.

A great deal of work and research has gone into the modeling of PM machines under DF conditions. Among these models, Finite Element Analysis (FEA) is widely used to analyze the operation of the machine due to its accuracy and reliability. In [1], the performance of a PM machine is analyzed in the presence of a crack in the PM. A computational time reduction methodology based on field reconstruction has been proposed to study the electromagnetic vibrations and torque ripples in PM machine with a partial DF [2].

Analytical modeling methods based on Fourier series expansion or Magnet Equivalent Circuit (MEC) methods are considered efficient and favorable due to their computational speed and acceptable accuracy. In [3], a study on magnetic fault signatures is presented, based on an analytical approach using MEC to determine the impact of the fault on the machine. The paper [4] presents a strategy for modeling an ER-PMSM with DF based on an improved MEC approach with dynamic responsibility while taking into account the saturation effect. An analytical model for predicting the air-gap field distribution is proposed by [5] using Halbach networks for an axial flux PM machine with partial DF. The authors of [6] provide a quantitative comparison of two sub-domain models for computing the magnetic field in PM machines with any combination of poles and slots. The magnetization vector is chosen using a model that considers the combined impact of slots and rotor topologies.

DF diagnosis is a critical research area for PM machines. [7] provides a mathematical model and FEA of a DF-operating machine. The analysis is employed for diagnosis by examining the spectrum signatures of the different demagnetization modes to explore the feasibility of a specific characterization created by the faults. In [8], a study of DF detection based on homopolar voltage measurement is proposed. The back Electromotive Force (EMF) is used to diagnosis this type of fault on inverter-powered machines, particularly for fault-tolerant systems. An investigation of the magnetic characteristics of a PM brushless DC motor demagnetization condition is presented

in [9]. The fault is diagnosis by measuring the radial magnetic field. The back-EMF and magnetic flux density are used to derive diagnosis accuracy as defect indices.

The main contribution of this paper is to propose an analytical approach to model the complete DF of two PMs for the ER-PMSM. The proposed analytical model requires less computational time and demonstrates good accuracy. The 2D FEA and experimental results are carried out to verify and validate the proposed model. The analytical approach is close to the real system and offers the advantages of an intuitive model and a distinct physical concept. In addition, this model can provide an accurate reference for fault diagnosis and preventive maintenance planning for the machine.

The paper is organized as follows: Section II presents the analytical model of the healthy and faulty ER-PMSM. In section III, a model validation using FEA. Finally, the robustness of the analytical model is demonstrated, followed by tests and experimental results.

II. Analytical Approach for ER-PMSM

In this paper, a 24-slot, 22-pole (24/22) three-phase ER-PMSM with a double-layer fractional-slot concentrated-wound (FSCW) structure is presented to verify the proposed method. A cross-section of the machine is depicted in Fig. 1. The parameters and dimensions of ER-PMSM are specified in Table I.

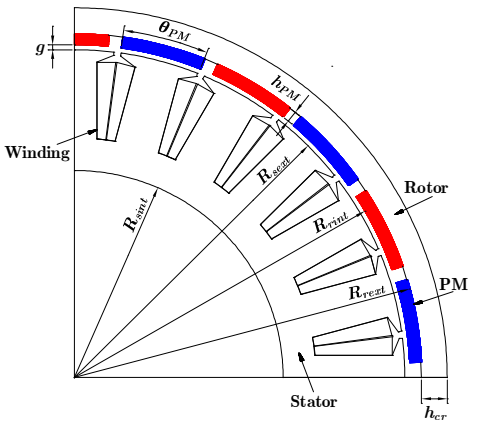

Fig. 1. Geometric parameters of the FSCW ER-PMSM.

TABLE I. ER-PMSM Parameters

Parameter	Value	Parameter	Value
Rated power P (kW)	1.5	Outer rotor radius R_{rext} (mm)	93
Rated speed ω (rpm)	600	Inner rotor radius R_{rint} (mm)	91.5
Frequency f (Hz)	110	Length L_{axe} (mm)	35
Rated current i_N (A_{RMS})	11	Air-gap length g (mm)	1.365
Rated torque Γ_e (N.m)	24	Magnet thickness h_{PM} (mm)	3
Number of slots N^s	24	Magnet arc θ_{PM} (°)	14
Number of poles $2p$	22	Rotor thickness h_{cr} (mm)	7
Number of turns per coil N_T	22	Magnet-arc to pole-pitch ratio α_p (%)	85.5
Magnet flux ϕ_{PM} (Wb)	0.1021	Residual flux density of PM B_r (T)	1.26
Outer stator radius R_{sext} (mm)	88.635	PM	NdFeB N38SH
Inner stator radius R_{sint} (mm)	56	Magnetic steel	M530-50A

In this study, the developed analytical calculation depends on the following assumptions:

(1) Infinite permeability of iron;

(2) The magnetic energy is concentrated in the air-gap;

(3) Small air-gap compared to the inner radius of the stator and the radial magnetic field (tangential magnetic fields are negligible).

A. Healthy ER-PMSM Model

a) PM Air-Gap Flux Density

Let's consider the flux density model of an FSCW PM motor presented in [10]. The flux density function generated by the PMs in the air-gap depends directly on:

- The residual flux density of PMs;
- The magnet arc angle of PMs;
- The geometrical dimensions of PMs;
- The positioning of the PMs in the rotor.

The general form of the flux density produced by the PMs in the air-gap is given by the following expression:

$$b^r(\alpha_r)=\begin{cases} -B_{PM} & \alpha_r \in \left[-\pi;-\frac{\alpha_m}{2}-\alpha_{na}\right]\cup\left[\frac{\alpha_m}{2}+\alpha_{na};\pi\right] \\ 0 & \alpha_r \in \left[-\frac{\alpha_m}{2}-\alpha_{na};-\frac{\alpha_m}{2}\right]\cup\left[\frac{\alpha_m}{2};\frac{\alpha_m}{2}+\alpha_{na}\right] \\ B_{PM} & \alpha_r \in \left[-\frac{\alpha_m}{2};\frac{\alpha_m}{2}\right] \end{cases} \quad (1)$$

$$B_{PM}=\frac{B_r h_m}{g+\left(h_m/\alpha_p\right)} \quad (2)$$

Where:

- α_{na} is the empty angle between two PMs;
- B_{PM} is the value of the flux density created by a PM in the air-gap;
- α_p is the coefficient of the polar arc of the PM, which is calculated by the following expression in our analysis $\alpha_p = \theta_{PM} / \tau_p$;
- τ_p is the pole pitch, $\tau_p = \pi / p$.

The rotor flux density, under pole pair, along the magnetization direction in rotor reference is represented by the waveform shown in Fig. 2.

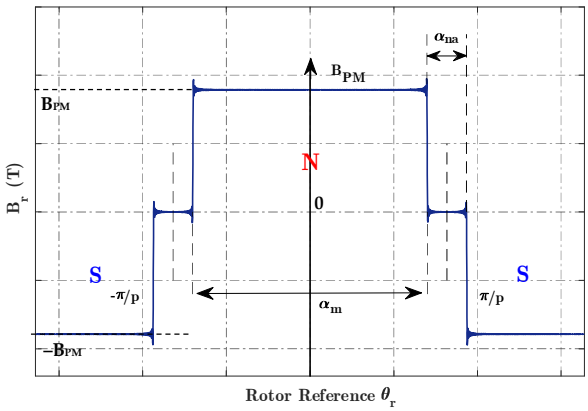

Fig. 2. Air-gap flux density generated by PM over a pole pitch.

The healthy distribution of the normal magnetic flux density generated by the PMs as a function of the rotor reference α_r can be defined in the following Fourier decomposition form:

$$b^r(\alpha_r) = \frac{4B_{PM}}{\pi}\sum_{h=0}^{+\infty}\left[\frac{1}{(2h+1)}\sin\left((2h+1)\frac{\alpha_m}{2}\right)\cdot\cos\left((2h+1)\alpha_r\right)\right] \quad (3)$$

Where $\alpha_r = \alpha_s - \theta = \alpha_s - ((\omega t/p) + \theta_0)$

b) Magnetic Flux

The calculation of the flux linkage generated by the PMs perceived by phase j depends on the winding distribution of the concerned phase. The elementary flux under the no-load case is derived by integrating the air-gap flux density.

$$\Phi_j(\theta) = N_T \iint b^r(\alpha_r)\, dS_j \quad (4)$$

We consider that the flux density created by the PMs is uniform and varies with the radius of the ER-PMSM and the winding distribution function $F_{distribution}$ [11]. The magnetic flux can be expressed as follows:

$$\Phi_j(\theta) = N_T R_{sext} L_{axe} \int_0^{2\pi} F_{distribution,j}(\alpha_s)\, b^r(\theta)\, d\alpha_s \quad (5)$$

The stator winding structure of the ER-PMSM is depicted in Fig. 3. Each phase is composed of 8 Elementary Coils (EC).

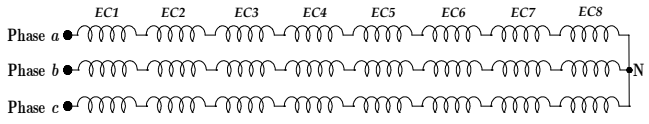

Fig. 3. Structure of the stator winding of the ER-PMSM.

The winding distribution function shown in Fig. 4 can be given by the following expression:

$$F_{distribution}(\alpha_s) = \sum_{h=0}^{+\infty}\left[\frac{4}{\pi(2h+1)}\left[\cos\left((2h+1)\theta_c\right) - \cos\left((2h+1)(2\theta_c - 1)\right)\right]\right] \cdot \sin\left((2h+1)\alpha_s\right) \quad (6)$$

Where θ_c is the coil opening angle, $\theta_c = 2\pi / N^s$.

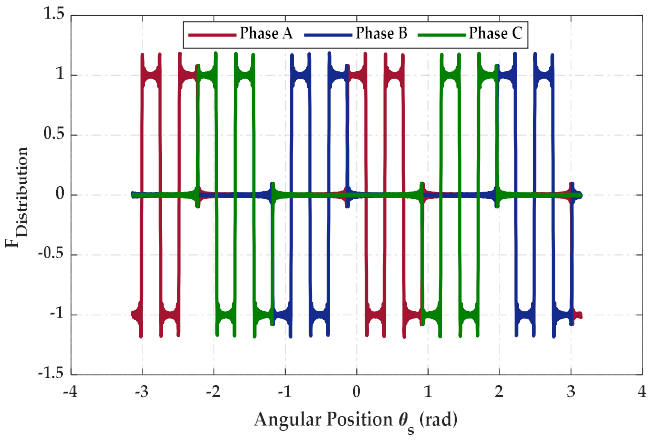

Fig. 4. Winding distribution function.

c) Back Electromotive Force

The no-load-back Electromotive Force (EMF) is determined by the variation of the flux through a coil using Faraday's law. When the rotor rotates by one polar step, a PM south pole takes the place of a PM north pole, and the flux in the coil reverses. The above developments concern the phase whose axis is along the reference axis. To obtain the expressions, they must be shifted relative to each other by an angle of $2\pi/3$. The back-EMF of each phase can be determined by the following expression:

$$E_j(t) = -\frac{d}{dt}\Phi_j(\theta) \quad (7)$$

Where $j = a, b, c$ represents, respectively, the phases a, b and c of the stator winding.

B. Faulty ER-PMSM Model

a) Faulty PM Air-Gap Flux Density

According to the machine model shown in Fig. 3, the faulty air-gap flux density is calculated from the healthy approach. The decomposition of the b^f is employed to illustrate the effect of the fault. The faulty flux density of a complete DF of two adjacent PMs can be expressed as follows:

$$b^{r,faulty}(\alpha_r) = b^r(\alpha_r) - b^f(\alpha_r) \quad (8)$$

$$b^f(\alpha_r) = \sum_{h=1}^{+\infty} B_h^f \cos\left(h\alpha_r + \varphi_h^f\right) \quad (9)$$

The analytical waveforms of the faulty PM air-gap flux density are shown in Fig. 5.

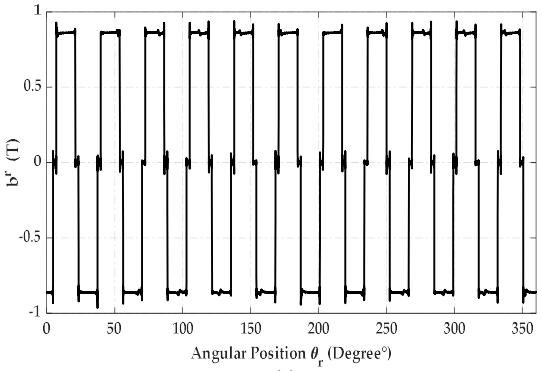

(a)

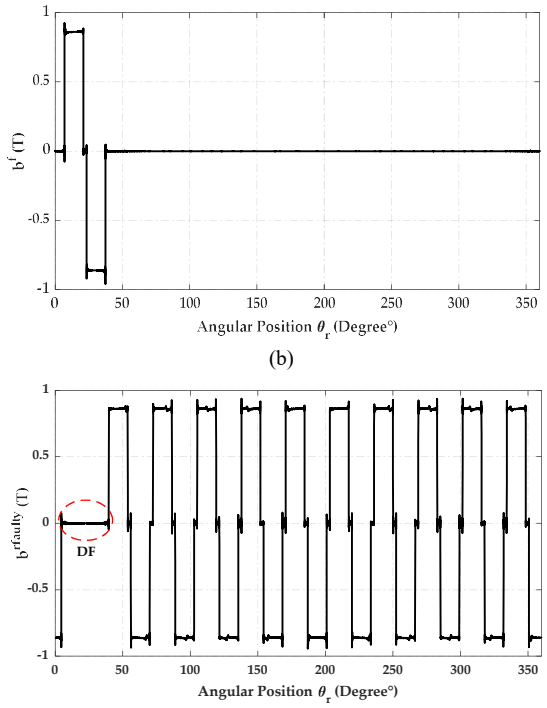

Fig. 5. The faulty air-gap flux density of the ER-PMSM, (a) Healthy state, (b) Flux density over two adajcent poles, (c) Faulty state.

b) Faulty Magnetic Flux

The flux generated by the PMs crosses each elementary coil. The flux through coils of the phases can be described by the following expressions:

$$\Phi_{j,faulty}(\theta) = N_T \iint b^{r,faulty}(\alpha_r)\, dS_j \tag{10}$$

$$\Phi_{j,faulty}(\theta) = N_T R_{sext} L_{axe} \int_0^{2\pi} F_{distribution,j}(\alpha_s)\, b^{r,faulty}(\theta)\, d\alpha_s \tag{11}$$

III. Numerical Validation: Finite Element Analysis

The FEA is widely used for in-depth analysis of electrical machines, enabling the intensity distribution of the flux density to be examined. This paper uses a numerical method to illustrate the impact of the full DF for the acquisition and analysis of magnetic signals. To evaluate the proposed analytical approach, a two-dimensional FEA-2D model of the ER-PMSM is considered. Simulations have been performed for the examined cases to illustrate and discuss the behavior of the healthy and faulty machine with a full DF of two adjacent PMs. The parameters of the ER-PMSM are given in Table I.

The distribution of the healthy and faulty flux densities is shown in Fig. 6. The flux density of the healthy model is higher and achieves satisfactory values without any extremely saturated regions. When the fault occurs, there is a significant decrease in the flux density, which can lead to a non-uniform distribution of the magnetic field lines and an asymmetry of the induced currents. The impact of the fault is shown in the flux line distribution presented in Fig. 7. Indeed, the missing flux produced by PMs is perceptible. It leads to a reduction in the voltage induced in the phases when the faulty PMs pass under the coil, which will generate an unbalance in the magnetic flux generated by the PMs and directly on the three-phase back-EMF.

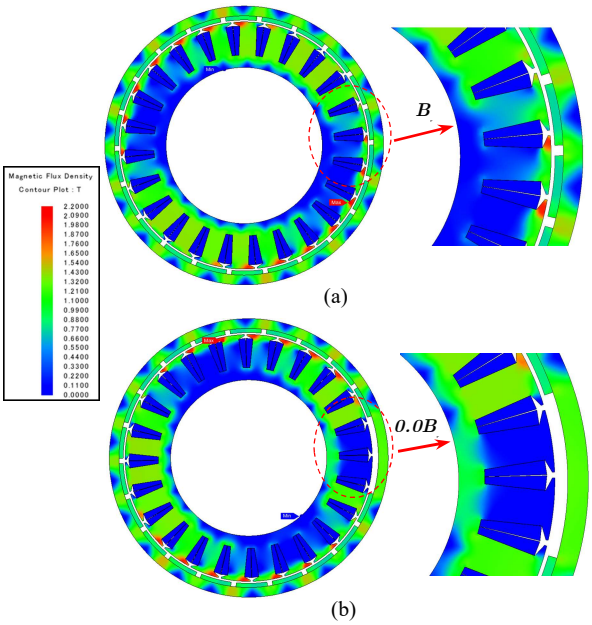

Fig. 6. The healthy and faulty flux density of the ER-PMSM at 5 N.m load and 600 rpm, (a) Healthy state, (b) Faulty state.

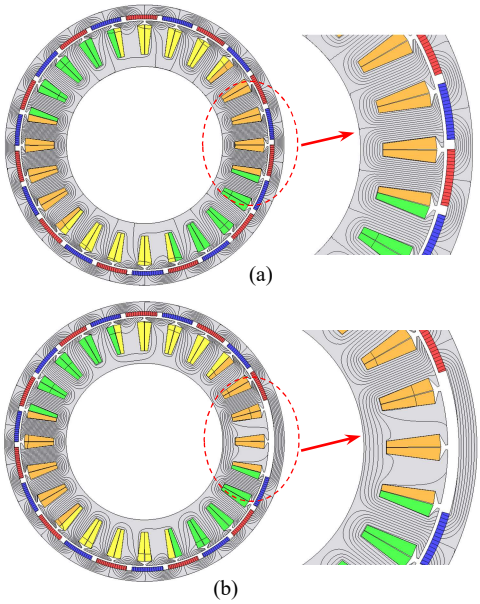

Fig. 7. The healthy and faulty flux line distribution of the ER-PMSM at 5 N.m load and 600 rpm, (a) Healthy state, (b) Faulty state.

The radial flux density in the air-gap determined by the analytical model and FEA in the healthy and faulty states is illustrated in Fig. 8 and Fig. 9. In the DF case, the fault has a significant impact on the flux density in the region of the missing PMs. The numerical results are consistent with the analytical approaches.

The results shown in Fig. 10, 11, 12, and 13 illustrate the no-load flux obtained using the analytical and FEA approaches at a speed of 600 rpm. Since the flux density generated by PMs is impacted by the fault, the ER-PMSM no-load flux varies proportionally, and its magnitude decreases by around 25% compared to the healthy condition. The impact of the fault on the motor is severe, reducing the back-EMF and leading to higher currents in the ER-PMSM windings, which can damage the winding insulation and affect the machine's performance. The no-load back-EMFs developed by the two methods are shown

in Fig. 14, 15, 16, and 17. Due to the fault, the no-load back-EMF induced by the flux variation in the windings changes accordingly, introducing a remarkable unbalance. In Fig. 18, the ER-PMSM operates at 5 Nm load, and the FEA representation of the torque waveform is provided. Under faulty conditions, the torque of the machine will be affected, and due to the change in the rotor symmetry, torque ripples appear.

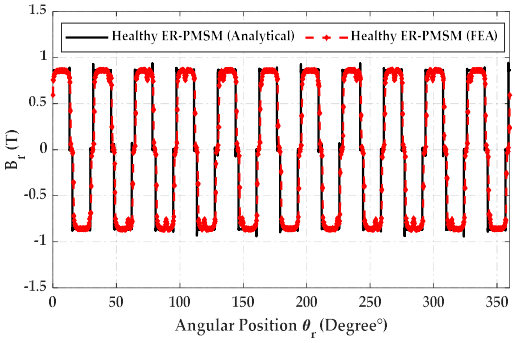

Fig. 8. The healthy PM air-gap flux density of the ER-PMSM.

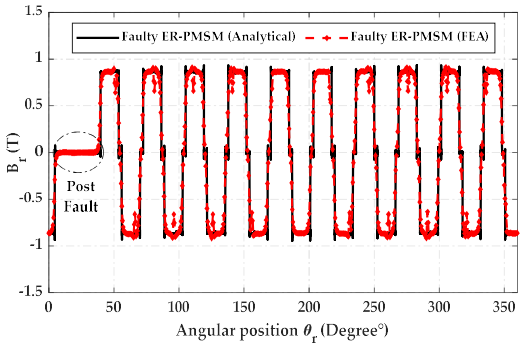

Fig. 9. The faulty PM air-gap flux density of the ER-PMSM.

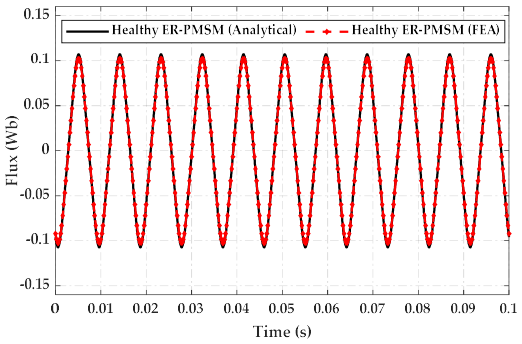

Fig. 10. he healthy flux linkage generated by PMs through phase *a*.

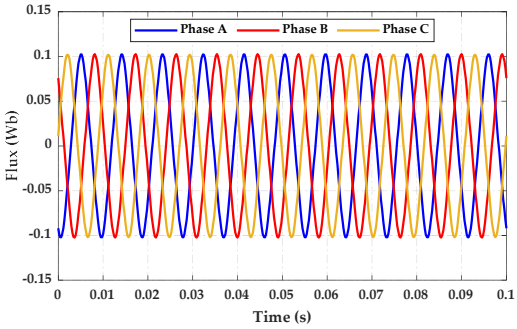

Fig. 11. The healthy flux linkage generated by PMs of the ER-PMSM.

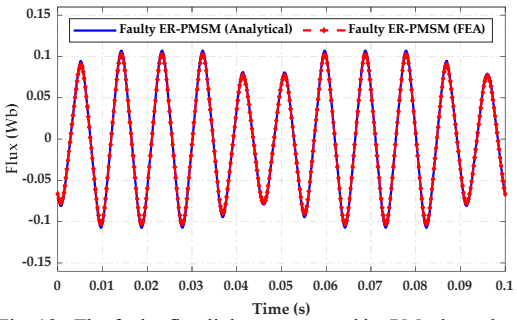

Fig. 12. The faulty flux linkage generated by PMs through phase *a*.

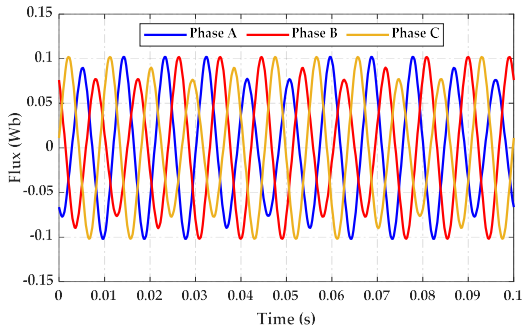

Fig. 13. The faulty flux linkage generated by PMs of the ER-PMSM.

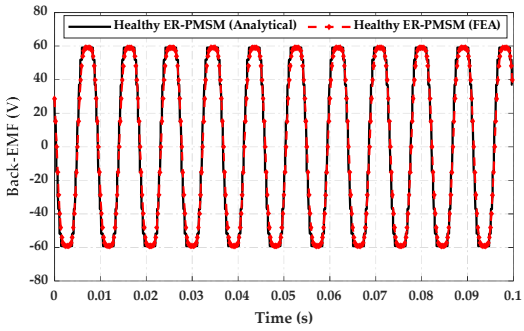

Fig. 14. The healthy back-EMF of phase *a*.

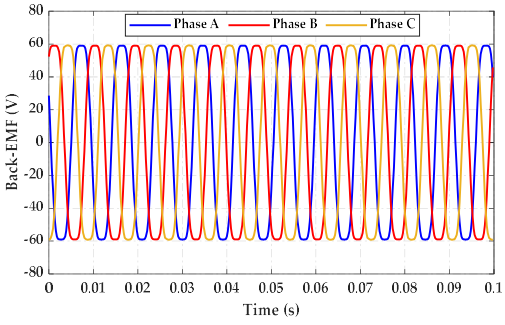

Fig. 15. The healthy back-EMF of the ER-PMSM.

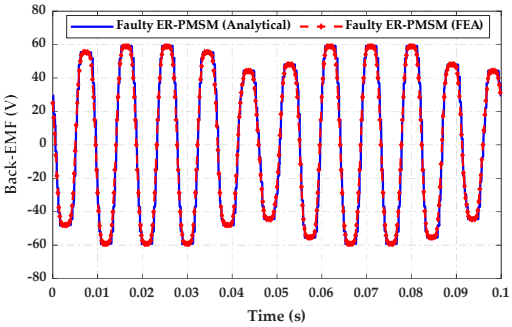

Fig. 16. The faulty back-EMF of phase *a*.

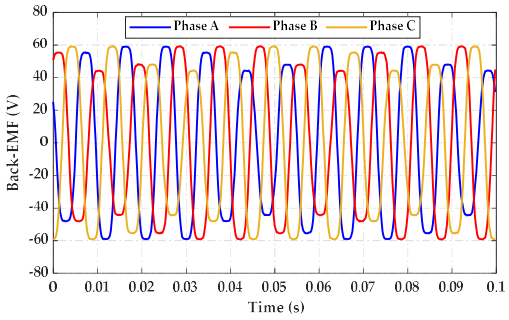

Fig. 17. The faulty back-EMF of the ER-PMSM.

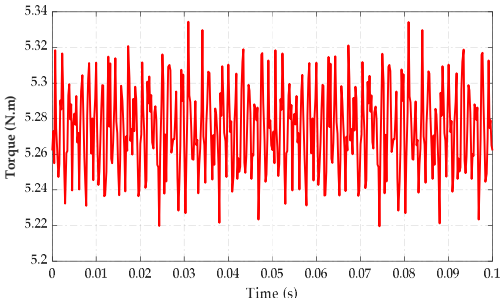

Fig. 18. The FEA faulty electromagnetic torque of the ER-PMSM.

IV. Experimental Setup and Verification

A. Demagnetization Fault Implementation

The experimental campaign has emphasized the prototype of the FSCW ER-PMSM with a DF to validate the results acquired analytically and by FEA. To carry out the study, the ER-PMSM has been designed to offer the possibility of realizing the fault with a rotor including two PMs that have been demagnetized by a thermal method. The assembly process is illustrated in Fig. 19.

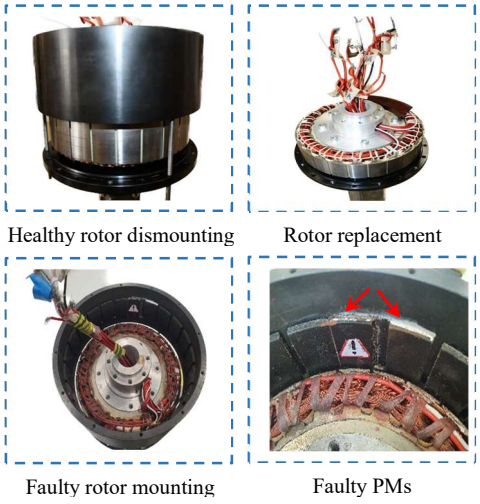

Fig. 19. Faulty rotor mounting of ER-PMSM prototype.

B. Experimental Platform

To validate the proposed approach, an experimental platform of ER-PMSM with DF is designed. As shown in Fig. 20, the test bench consists of the ER-PMSM coupled to the load machine and its Semikron three-phase IGBT inverter. The control is performed via a dSpace-MicroLabBox 1202 system. The electromagnetic torque is measured via a T22 sensor connected to an HBM MX440B amplifier module.

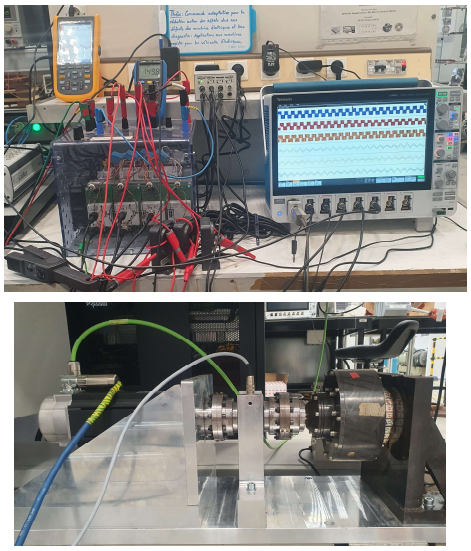

Fig. 20. Experimental test bench.

Measurement of healthy and faulty back-EMF is performed using a drive motor at 600 rpm (Fig. 21, 22). The results of the analytical and FEA models correspond to the experimental results. However, there is a slight discrepancy between the analytical, FEA, and measured results, which can be potentially due to the manufacturing process. The faulty electromagnetic torque under FEA is experimentally validated as shown in Fig. 23. As a result, the calculations and approaches are validated. By comparing the measurement torque in the faulty case at 600 rpm and 5N.m load with the numerical simulation, it can be shown that the results match well.

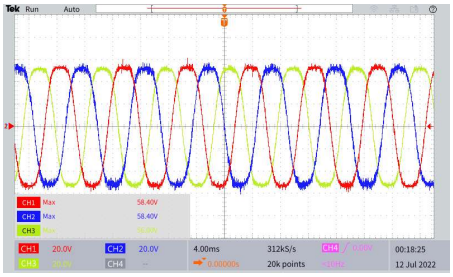

Fig. 21. The experimental healthy back-EMF of the ER-PMSM.

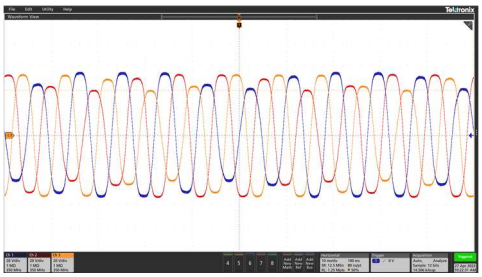

Fig. 22. The experimental faulty back-EMF of the ER-PMSM.

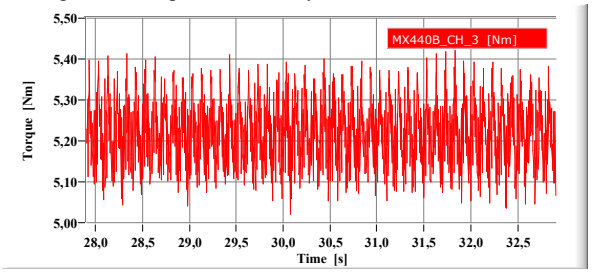

Fig. 23. The experimental faulty torque of the ER-PMSM.

V. Conclusion

This paper presents an approach to the analytical modeling of an ER-PMSM with a full demagnetization fault in two adjacent PMs. This modeling technique based on the demagnetization region is also applicable to various types of demagnetization faults. This model enables us to examine the theoretical performance of different operating conditions. Flux density, flux linkage, back-EMF, and torque have been developed under healthy and demagnetization situations. These parameters are quickly calculated with good accuracy compared with the FEA and experimental results. The proposed methodologies offer significant advantages, such as fast computation and correlations between several components. The analytical and numerical study will highlight the presence of fault components, provide information on the state of the ER-PMSM, and thus identify possible failure levels. Using this analytical development, a fault tolerant control strategy, fault detection, and diagnosis can be implemented in numerical models (such as MATLAB/Simulink) to provide a reference for the prediction and planning of the maintenance.

References

[1] R. Ginzarly, K. Alameh, G. Hoblos, and N. Moubayed, "Numerical versus analytical techniques for healthy and faulty surface permanent magnet machine," in 2016 Third International Conference on Electrical, Electronics, Computer Engineering and their Applications (EECEA), Apr. 2016, pp. 83–87. doi: 10.1109/EECEA.2016.7470770.

[2] D. Torregrossa, A. Khoobroo, and B. Fahimi, "Prediction of Acoustic Noise and Torque Pulsation in PM Synchronous Machines With Static Eccentricity and Partial Demagnetization Using Field Reconstruction Method," IEEE Trans. Ind. Electron., vol. 59, no. 2, pp. 934–944, Feb. 2012, doi: 10.1109/TIE.2011.2151810.

[3] M. Zafarani, T. Goktas, and B. Akin, "A Comprehensive Analysis of Magnet Defect Faults in Permanent Magnet Synchronous Motors," IEEE Trans. Ind. Appl., pp. 1–1, 2015, doi: 10.1109/TIA.2015.2487440.

[4] S. Sharouni, P. Naderi, M. Hedayati, and P. Hajihosseini, "Demagnetization fault detection by a novel and flexible modeling method for outer rotor permanent magnet synchronous machine," Int. J. Electr. Power Energy Syst., vol. 116, p. 105539, Mar. 2020, doi: 10.1016/j.ijepes.2019.105539.

[5] B. Guo, Y. Huang, F. Peng, and J. Dong, "General Analytical Modeling for Magnet Demagnetization in Surface Mounted Permanent Magnet Machines," IEEE Trans. Ind. Electron., vol. 66, no. 8, pp. 5830–5838, Aug. 2019, doi: 10.1109/TIE.2018.2873099.

[6] Z. Q. Zhu, L. J. Wu, and Z. P. Xia, "An Accurate Subdomain Model for Magnetic Field Computation in Slotted Surface-Mounted Permanent-Magnet Machines," IEEE Trans. Magn., vol. 46, no. 4, pp. 1100–1115, Apr. 2010, doi: 10.1109/TMAG.2009.2038153.

[7] J. I. Melecio, S. Djurović, and N. Schofield, "FEA model study of spectral signature patterns of PM demagnetisation faults in synchronous PM machines," J. Eng., vol. 2019, no. 17, pp. 4127–4132, Jun. 2019, doi: 10.1049/joe.2018.8048.

[8] J.-C. Urresty, J.-R. Riba, and L. Romeral, "A Back-emf Based Method to Detect Magnet Failures in PMSMs," IEEE Trans. Magn., vol. 49, no. 1, pp. 591–598, Jan. 2013, doi: 10.1109/TMAG.2012.2207731.

[9] A. Usman, V. K. Sharma, and B. S. Rajpurohit, "Condition monitoring and severity estimation of rotor demagnetisation fault using magnetic flux measurement data," IET Energy Syst. Integr., vol. 3, no. 4, pp. 437–450, Dec. 2021, doi: 10.1049/esi2.12024.

[10] Z. Q. Zhu and Y. Liu, "Analysis of Air-Gap Field Modulation and Magnetic Gearing Effect in Fractional-Slot Concentrated-Winding Permanent-Magnet Synchronous Machines," IEEE Trans. Ind. Electron., vol. 65, no. 5, pp. 3688–3698, May 2018, doi: 10.1109/TIE.2017.2758747.

[11] A. Belkhadir, R. Pusca, D. Belkhayat, R. Romary, and Y. Zidani, "Analytical Modeling, Analysis and Diagnosis of External Rotor PMSM with Stator Winding Unbalance Fault," Energies, vol. 16, no. 7, p. 3198, Apr. 2023, doi: 10.3390/en16073198.

Authors' Information

Ahmed Belkhadir received the M.S. degree in electrical engineering and renewable energy in 2020 from Cadi Ayyad University, Marrakesh, Morocco. He is actually pursuing Ph.D. studies in the Laboratory of Electrical Systems and Environment (LSEE), Artois University, Béthune, France, and the Laboratory of Electrical Systems, Energy Efficiency and Telecommunications (LSEEET), Cadi Ayyad University, Marrakesh, Morocco. His research interest concerns the control and diagnosis of electrical machines.

Remus Pusca was born in Medias, Romania, in 1972. He received his Dipl. Ing. and M.S. degree in electrical engineering from the Technical University of Cluj-Napoca (UTCN), Cluj-Napoca, Romania, in 1995 and 1997, respectively. From 1997 to 1998, he was an Assistant Research Worker with the Department of Heat Treatment and Thermal Equipment, UTCN. From 1999 to 2003, he was a Research Worker with the Centre Recherche Electrotechnique Electronique Belfort. He obtained his Ph.D. degree in Electrical Engineering from the University of Franche-Comté, France in 2002. Since 2003, he is Assistant Professor at University of Artois, and a Member of the Team Research of the Laboratory of Electrical Systems and Environment (LSEE), Bethune, France. His knowledge in the field of diagnosis applied to electric machines were developed by working with the LSEE team specialized in this field. His current research interests include control of electrical systems and diagnosis of electrical machines.

Raphaël Romary (Member, IEEE) received the Ph.D. from Lille University, Lille, France, in 1995 and the D. SC degree from Artois University, Béthune, France, in 2007. He is currently a Full Professor in Artois University and a Researcher at the Laboratory of Electrical Systems and Environment (LSEE). His research interest concerns the analytical modeling of electrical machines with applications to noise and vibration, losses, electromagnetic emissions, diagnosis.

Driss Belkhayat was born in 1967 in Fez, Morocco. He did his graduate studies at Orsay University (PARIS XI) before continuing at the Ecole Normale Supérieure of Cachan in Paris. He received his PhD in 1993 from LILLE I University. In 2004, he received his State PhD in Electrical Engineering in his native country at Cadi Ayyad University (UCA) in Marrakesh. He is currently a Full Professor in Cadi Ayyad University, Researcher and Director of the Laboratory of Electrical Systems, Energy Efficiency and Telecommunications (LSEEET) of the Faculty of Sciences and Techniques of Marrakesh and Director of InnovTech doctoral center grouping 20 UCA research structures. His research field concerns electrical machines noise and vibrations reduction, numerical modeling and theoretical approaches by oriented control, the diagnosis and machine control methods.

Youssef Zidani was born in 1972, he received in 1994 his Diploma of Hight School Teachers degree in Electrical Engineering from ENSET (Rabat, Morocco). In 1997 and 2004 he received respectively the MSA and PhD degrees in Electrical Engineering and Power Electronics from Mohamed V University (Mohammadia School of Engineers, EMI, Rabat). In 2017, he received the Habilitation diploma from Cadi Ayad University. From 1994-2004, he was an Assistant Professor at Hight School of Technology (EST, Mohamed 1st University, Oujda). In 2004, he joined the Department of Applied Physics in the Faculty of Science and Technology (FST, Cadi Ayad University, Marrakesh) where he is actually a permanent Professor. His research interests are Electrical machines, Power electronics and Renewable energy.

Abderrahmane Rebhaoui was born in Algiers, Algeria, in 1994. He received the Engineer Diploma degree in Electrical Engineering from Ecole Nationale Polytechnique, Algiers, in 2018. He received the MSc degree from the University of Le Havre Normandie, France, in 2019. He joined Institut VEDECOM, Versailles – France, In 2019, as a Ph.D. Student, in collaboration with Laboratoire Systèmes Electrotechniques et Environnement (LSEE), Artois University, France. His research work focuses on electric motor design, magnetic material characterization and optimization.